REPORT

NEURODEVELOPMENT

Multicluster Pcdh diversity is required for mouse olfactory neural circuit assembly

George Mountoufaris,[1,2]† Weisheng V. Chen,[1,2]*† Yusuke Hirabayashi,[2,3] Sean O'Keeffe,[1,2] Maxime Chevee,[1,2] Chiamaka L. Nwakeze,[1,2] Franck Polleux,[2,3] Tom Maniatis[1,2]‡

The vertebrate clustered protocadherin (Pcdh) cell surface proteins are encoded by three closely linked gene clusters (*Pcdh*α, *Pcdh*β, and *Pcdh*γ). Here, we show that all three gene clusters functionally cooperate to provide individual mouse olfactory sensory neurons (OSNs) with the cell surface diversity required for their assembly into distinct glomeruli in the olfactory bulb. Although deletion of individual *Pcdh* clusters had subtle phenotypic consequences, the loss of all three clusters (tricluster deletion) led to a severe axonal arborization defect and loss of self-avoidance. By contrast, when endogenous Pcdh diversity is overridden by the expression of a single–tricluster gene repertoire (α and β and γ), OSN axons fail to converge to form glomeruli, likely owing to contact-mediated repulsion between axons expressing identical combinations of Pcdh isoforms.

The vertebrate clustered protocadherin *Pcdh*α, *Pcdh*β, and *Pcdh*γ genes (Fig. 1) generate a high level of cell surface diversity in the nervous system by a mechanism of stochastic promoter choice (*1*, *2*) and assembly of α, β, and γ protein monomers into combinatorial cis homo- or heterodimers that engage in homophilic interactions at the cell surface (*3*–*5*). Functional studies in mice revealed that the *Pcdh*γ gene cluster is required for dendritic self-avoidance in retinal starburst amacrine cells (*6*). However, it remains unclear why a self-avoidance phenotype was not observed in most other neuronal cell types examined in either *Pcdh*γ (*7*–*11*) or *Pcdh*α (*12*) single cluster deletion mutant mice.

Here, we address the functional significance of the multicluster organization of *Pcdh* genes, focusing on the wiring of mouse olfactory sensory neurons (OSNs). Individual OSNs monoallelically express a single olfactory receptor (OR) (referred to as "like-OSNs") (*13*, *14*) and project their axons to the olfactory bulb (OB) to form glomeruli (*15*). RNA-sequencing analysis of bulk (fig. S1A), as well as individual, OSNs (Fig. 1) (*16*, *17*) revealed that individual mature OSNs (mOSNs) stochastically express distinct combinations of alternate Pcdh isoforms from all three gene clusters. However, unlike the Purkinje cells (*18*) in which both alternate and C-type isoforms are expressed, the C-type Pcdh isoforms were detected in only a small fraction of mOSNs (Fig. 1 and tables S1 and S2). Moreover, both alternate and C-type isoforms were expressed in immature OSNs (fig. S1A). Thus, the C-type Pcdh isoforms are selectively down-regulated during OSN maturation.

To determine the function of the entire *Pcdh* gene cluster in OSN wiring, we generated mice in which the 1 million base pairs of DNA spanning all three gene clusters were deleted (*Pcdh*α, *Pcdh*β, *Pcdh*γ–tricluster deletion) (figs. S2 and S3). Because of the neonatal lethality of the tricluster-deletion pups, our analyses were carried out at postnatal day 0 (Fig. 2). A severe protoglomerular (glomeruli of newborns) phenotype was observed in the *Pcdh* tricluster deletion mice (Fig. 2, A to C). Although, most like-*Pcdh*–null OSN axons converged to their approximately normal coordinates in the bulb, they failed to form normal-appearing protoglomeruli (fig. S4A). To visualize the effect of the tricluster deletion on individual OSNs, they were labeled by using an in utero electroporation method adapted for the olfactory epithelium (fig. S5A), and their morphology was examined as they project to the bulb. As shown in Fig. 2G, individual OSN axons in the tricluster deletion neonates did not display the normal "cup"-shaped axonal arbors observed in control mice. Rather, mutant axonal arbors appeared heavily clumped and distorted, indicative of the loss of self-avoidance, resulting in the formation of abnormal protoglomeruli (Fig. 2, G and H, and fig. S5, B to E).

We next generated mice in which each of the *Pcdh* gene clusters was deleted (fig. S2). By contrast to the severe phenotype observed in the tricluster-deletion mice, deletion of the *Pcdh*α gene cluster led to the appearance of somewhat less compact protoglomeruli, consistent with a previous report of *Pcdh*α hypomorphic mice (*19*) (Fig. 2D). In addition, no major discernible defect in protoglomeruli formation was found when either the *Pcdh*β or *Pcdh*γ gene cluster was deleted, as compared with the mice having a tricluster deletion (Fig. 2, A to F, and see material and methods). Taken together, these deletion studies indicate that, in the complete absence of multicluster Pcdhs, "sister" axonal arbors from individual OSNs fail to recognize self and thus display the clumped phenotype. However, in the absence of the *Pcdh*α or *Pcdh*β or *Pcdh*γ gene cluster alone, the remaining two gene clusters provide individual OSNs with sufficient cell surface

[1]Department of Biochemistry and Molecular Biophysics, Columbia University, New York, NY 10032, USA. [2]Mortimer B. Zuckerman Mind Brain Behavior Institute, Columbia University, New York, NY 10032, USA. [3]Department of Neuroscience, Kavli Institute for Brain Science, Columbia University, New York, NY 10032, USA.
*Present address: Kallyope, Inc., New York, NY 10016, USA.
†These authors contributed equally to this work.
‡Corresponding author. Email: tm2472@cumc.columbia.edu

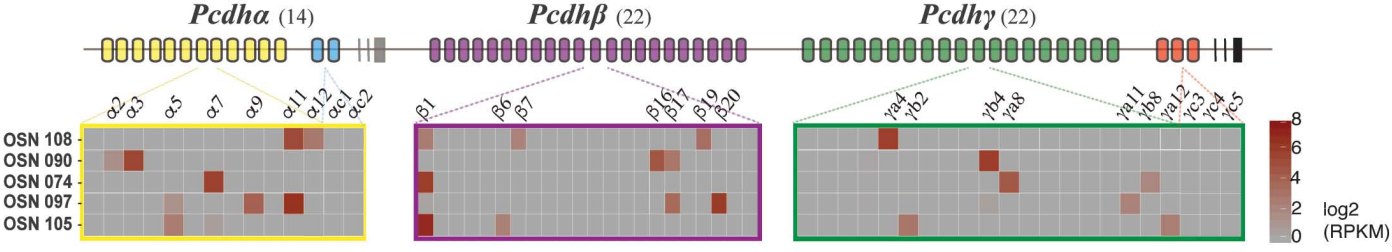

Fig. 1. Distinct combinations of Pcdhα, -β, and -γ isoforms are stochastically expressed in individual OSNs. Pcdh isoforms are divided into two categories, the alternate (indicated by the yellow, purple, and green ovals) and the C-type (indicated by the blue and red ovals). Single-cell, stochastic expression of Pcdhα and -β and -γ isoforms in five different mOSNs. Note the absence of detectable *Pcdh*α or -γ c-type expression in these cells (see tables S1 and S2). The presence of individual Pcdh isoform mRNA is indicated by red-colored boxes, and the levels are indicated by the color gradient [$\log_2$ reads per kilobase of transcript per million mapped reads (RPKM)].

diversity required for self-recognition and the formation of protoglomeruli.

To further explore the role of multicluster Pcdh diversity in olfactory circuit assembly, we established an OSN-cell–autonomous gain-of-function approach. Specifically, we sought to override the endogenous multicluster Pcdh single-cell diversity by expressing high levels of either one of two distinct sets of three Pcdh isoforms (α and β and γ) (uni-Pcdhs) (UNI1 and UNI3) (fig. S6, A and B, and fig. S12) exclusively in mOSNs. We found that the ectopic expression of the uni-Pcdh cassette did not affect OR choice (fig. S14), OR expression (fig. S13A), or OSN maturation (fig. S13B). However, a striking phenotype was observed in whole mounts and coronal sections of the olfactory bulbs of the uni-identity mice (both in UNI1 and UNI3): the absence of glomeruli in the olfactory bulb (Fig. 3 and fig. S6, B and D). Thus, the normal axonal interactions required for the postnatal assembly of glomeruli do not occur when the endogenous Pcdh diversity of individual OSNs was replaced with a single-tricluster Pcdh identity.

We next asked whether OSNs expressing the uni-Pcdh cassettes project to their normal sites of glomerulus formation in the OB. Specifically, we examined three different OSN populations that form glomeruli at distinct locations in the bulb by directly crossing the uni-identity mice to OR-specific reporter lines. We found that, in adult animals, OSN axons expressing the same OR, as well as the same set of Pcdhα and -β and

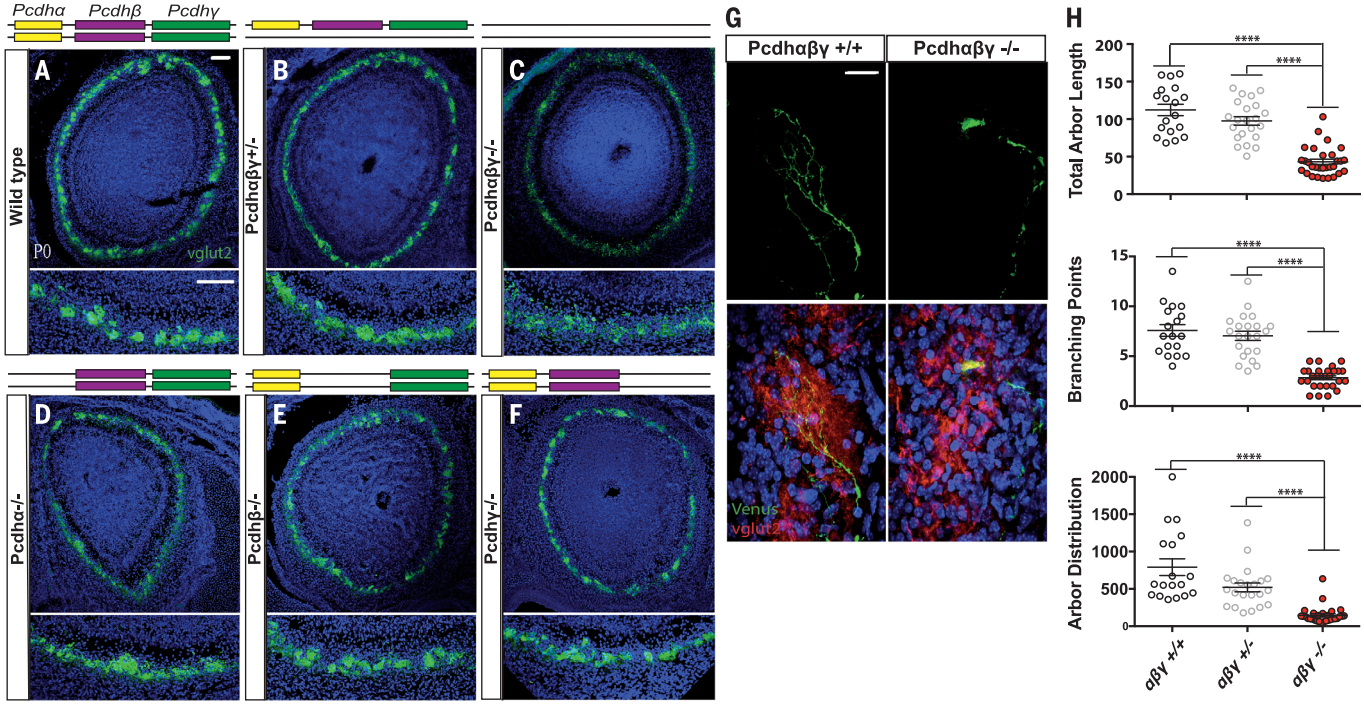

Fig. 2. Multiple *Pcdh* gene clusters are required for normal OSN axonal arborization and the formation of normal protoglomeruli. (**A**) Immunohistochemistry (IHC) against vesicular glutamate transporter 2 (*vglut2*) gene expression in coronal sections through the anterior OB of (A) wild-type, (**B**) *Pcdh*αβγ$^{+/-}$, (**C**) *Pcdh*αβγ$^{-/-}$, (**D**) *Pcdh*α$^{-/-}$, (**E**) *Pcdh*β$^{-/-}$, and (**F**) *Pcdh*γ$^{-/-}$ pups. Coronal section of the entire anterior bulb (top) and a zoomed-in area (bottom) through the OB. The three *Pcdh* gene clusters are indicated by the colored boxes. (**G**) IHC against Venus and vglut2 in utero electroporated OSNs from control and *Pcdh*αβγ$^{-/-}$ mice. (**H**) Quantification of the total length, the number of branch points, and the two-dimensional distribution of OSN arbors in *Pcdh*αβγ$^{+/+}$ (n = 18), *Pcdh*αβγ$^{+/-}$ (n = 22), and *Pcdh*αβγ$^{-/-}$ mice (n = 32) ($n \geq 6$ pups per genotype; Kruskal-Wallis test, $P < 0.0001$). Error bars represent SEM. DAPI, 4′,6-diamidino-2-phenylindole (blue). All Pcdh-tricluster mutant mice bear also the bacterial artificial chromosome Tg (see fig. S2). Scale bars: (A) to (F), 100 μm; and (G), 20 μm.

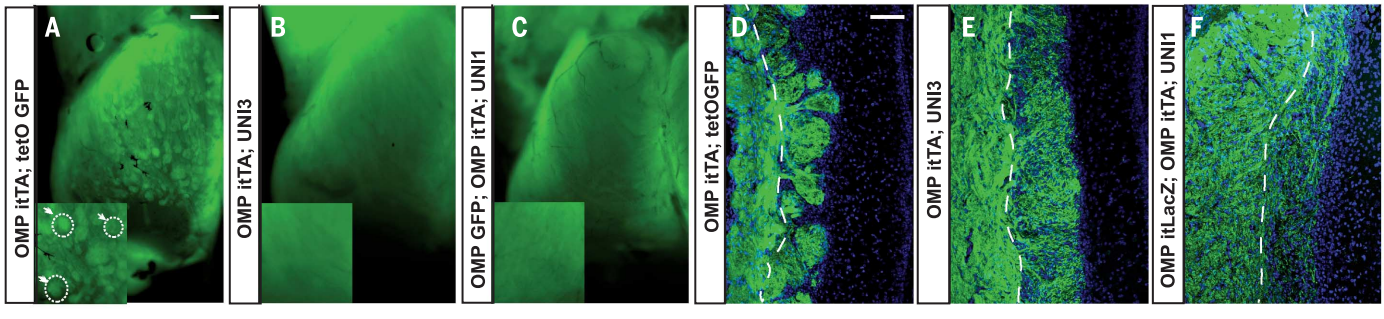

Fig. 3. Uni-identity OSN axons fail to form glomeruli. Whole-mount fluorescence microscopy images of the dorsal OB in (**A**) control and (**B** and **C**) uni-identity 4- to 5-week-old mice (mouse strains on figure). Arrows and circles highlight glomeruli in whole-mount zoom images. IHC against GFP, TagT, and β-galactosidase (β-Gal) in a coronal section through the OB in (**D**) control and (**E** and **F**) uni-identity 4- to 5-week-old mice. Dashed line designates the separation of the nerve layer (NL, left side) and the glomerular layer (GL, right side). TagT and β-Gal are pseudo-colored green; DAPI, blue. Scale bars: (A) to (C), 500 μm; (D) to (F), 100 μm.

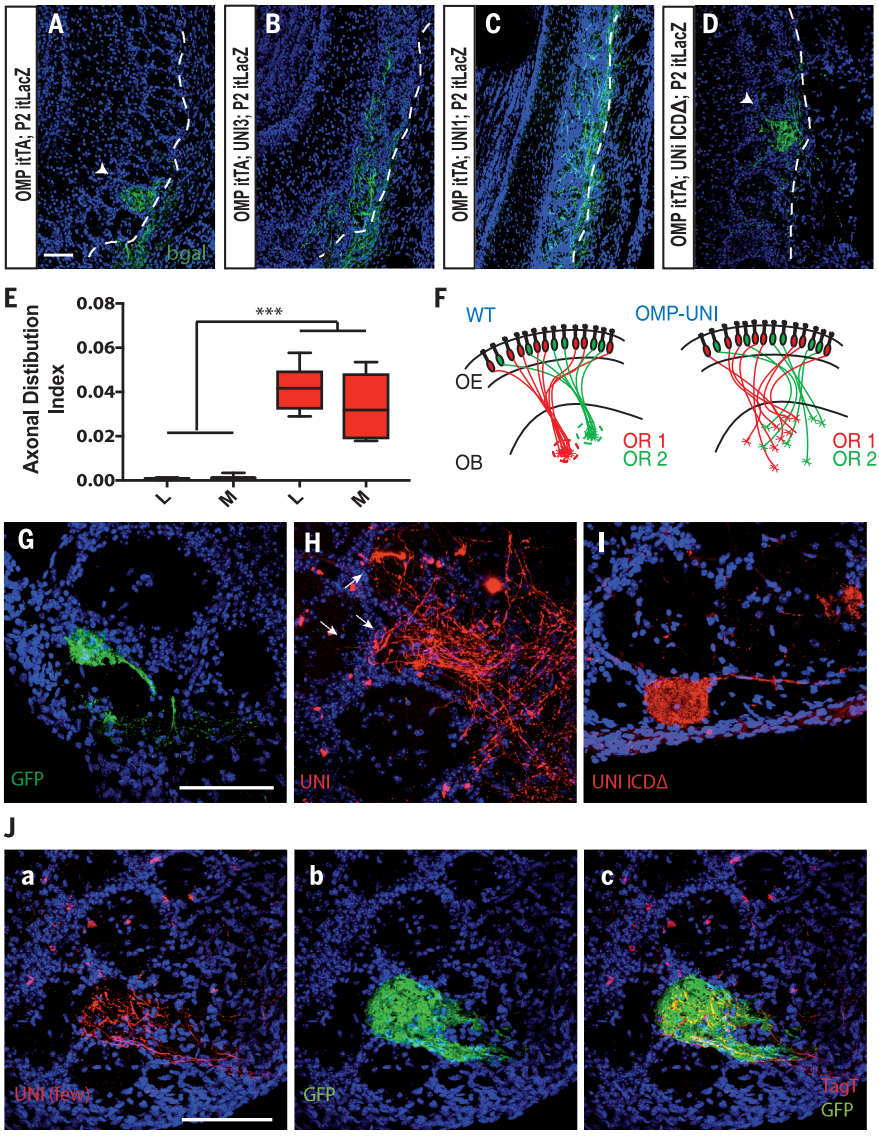

Fig. 4. Uni-identity like-OSN axons fail to converge in the OB. IHC against β-Gal in coronal sections through the OB in (**A**) control, (**B** and **C**) uni-identity, and (**D**) UNI ICDΔ in 4-week-old mice. Arrows depict the P2 medial glomerulus. Dashed line designates the separation of NL (right) and GL (left). β-Gal is pseudo-colored green. (**E**) Quantification of P2 axonal distribution of lateral and medial projections in the OB of 8-week-old control (black, $n = 9$ bulbs), and uni-identity mice (red, $n = 6$ bulbs). (Mann-Whitney test, medial $P = 0.0002$, lateral $P = 0.0004$). (**F**) Normally, like-OSN axons (OR1, red, and OR2, green) converge into stereotypically positioned glomeruli within the OB (left). OE, olfactory epithelium. In uni-identity mice, OSN axons that share the same single dominant Pcdh uni-identity project diffusely to their expected positions in the OB (right). (**G**) Expression of GFP or (**H**) UNI3, or (**I**) UNI ICDΔ cassette exclusively in MOR28 OSNs. Arrows depict the aberrant projection of MOR28-UNI axons in the bulb. [**J** (**a** to **c**)] The few MOR28-UNI axons localize with wild-type MOR28 OSNs labeled with GFP. Animals were 4 to 5 weeks old. DAPI, blue. Scale bar, 100 μm.

-γ isoforms (uni-Pcdhs), projected diffusely to their approximately normal stereotypic locations in the bulb but failed to organize into distinct glomeruli (Fig. 4, A to C; fig. S7; and fig. S8, B and C). Moreover, this lack of axonal convergence (Fig. 4, E and F) persisted throughout development, suggesting that uni-Pcdh–expressing axons have reached their "final" destinations in the OB (fig. S8A). Considering the absence of normal glomeruli in uni-identity mice, it was surprising to find that they were not anosmic (fig. S9, C and D). However, the uni-identity mice did display defects in odor discrimination (fig. S9, A and B). We note that the uni-identity OSN wiring phenotype required intact full-length Pcdh proteins, as apparently normal glomeruli were observed when the uni-Pcdh cassette was replaced with truncated Pcdh mutant isoforms in which either the extracellular domains (UNI ECDΔ) [required for homophilic interactions (*3*)] (fig. S11) or the intracellular domains (UNI ICDΔ) [thought to mediate intracellular signaling (*20*)] were deleted (Fig. 4D and fig. S10, A to C).

To address the selectivity and the underlying mechanism by which the uni-identity phenotype emerges, we examined the effect of overriding endogenous Pcdh diversity exclusively in like-OSNs, i.e., those expressing the same OR (e.g., the MOR28 receptor). In this case, if the presence of uni-Pcdhs mediates repulsion between individual OSN axons, the formation of MOR28-specific glomeruli should be prevented, without interfering with the assembly of all other glomeruli. We generated mice in which the majority of MOR28 OSNs expressed uni-Pcdh's, whereas other types of OSNs expressed only the endogenous Pcdh's. As predicted, MOR28-UNI axons failed to converge to form a glomerulus but instead spread into the territories of adjacent wild-type glomeruli (Fig. 4H). By comparison, control MOR28 OSN axons formed normal-appearing glomeruli (Fig. 4, G and I). These data substantiate the hypothesis that, as individual MOR28 OSN axons ("like-axons") expressing the same uni-Pcdhs converge to a common site in the bulb, they inappropriately recognize each other as being axons of the same neuron. As a consequence, Pcdh-mediated contact-dependent repulsion likely occurs between these like-axons and thus prevents them from converging to form a glomerulus.

We next examined animals expressing the uni-Pcdhs in only a limited number of MOR28 OSNs. We hypothesized that the presence of large numbers of wild-type MOR28 axons, each with its own Pcdh identity, would substantially "dilute" the uni-identity axons and, in essence, rescue or diminish the convergence phenotype (i.e., by minimizing the likelihood that MOR28-UNI axons will encounter each other during axonal convergence and glomerulus assembly) (fig. S15B). Indeed, as shown in Fig. 4J, the small number of MOR28-UNI axons project to the "right" location in the bulb [detected by the green fluorescent protein–positive (GFP+) wild-type axons] and form a close-to-normal glomerulus. These results show that the severity of the convergence defect of MOR28-UNI axons increases as larger numbers of interacting axons sharing the same Pcdh identity converge on the site of glomerulus formation (fig. S15C). More important, this observation is consistent with the notion that individual OSN axons displaying the same set of Pcdhα, -β, and -γ isoforms repel each other because of inappropriate Pcdh-dependent self-avoidance.

Here, we demonstrate that the mouse *Pcdhα*, *Pcdhβ*, and *Pcdhγ* gene clusters functionally complement each other to provide individual OSNs with sufficient levels of Pcdh cell surface diversity required for OSN wiring. This observation likely explains the lack of widespread neuronal wiring defects in mice bearing single–*Pcdh* gene–cluster deletions (*7*–*11*). Our studies also highlight the surprisingly similar logic by which the mouse clustered Pcdh and *Drosophila* Down syndrome cell adhesion molecule (Dscam) proteins function in analogous structures in the olfactory system. In both cases, loss of function leads to "clumping" of OSN axon termini during

glomeruli formation (*21*), whereas loss of single-cell diversity results in the absence of normal glomerular structures (*22*).

In addition, our observations reveal different modes of *Pcdh* gene regulation that depend on the identity of the expressing neuron: the stochastic expression of variable exons in the case of mOSNs and a deterministic expression of *Pcdhac2* in serotonergic neurons (*23*). This differential *Pcdh* gene expression likely reflects the unique requirement for normal wiring of the two neuronal cell types. In the case of olfactory neurons, multicluster diversity in *Pcdh* expression is required for convergence of like-axons to form glomeruli. By contrast, serotonergic neurons express the same C-type isoform, which mediates homotypic axonal repulsion, ensuring even distribution of their axon termini in the brain (*23*). Thus, the same multiclustered *Pcdh* gene family functions in glomeruli formation by olfactory neurons and tiling by serotonergic neurons, providing a remarkable example of functional diversification of a gene family accomplished simply by the evolution of distinct transcriptional programs.

REFERENCES AND NOTES

1. B. Tasic *et al*., *Mol. Cell* **10**, 21–33 (2002).
2. X. Wang, H. Su, A. Bradley, *Genes Dev.* **16**, 1890–1905 (2002).
3. R. Rubinstein *et al*., *Cell* **163**, 629–642 (2015).
4. D. Schreiner, J. A. Weiner, *Proc. Natl. Acad. Sci. U.S.A.* **107**, 14893–14898 (2010).
5. C. A. Thu *et al*., *Cell* **158**, 1045–1059 (2014).
6. J. L. Lefebvre, D. Kostadinov, W. V. Chen, T. Maniatis, J. R. Sanes, *Nature* **488**, 517–521 (2012).
7. W. V. Chen *et al*., *Neuron* **75**, 402–409 (2012).
8. A. M. Garrett, D. Schreiner, M. A. Lobas, J. A. Weiner, *Neuron* **74**, 269–276 (2012).
9. J. Ledderose, S. Dieter, M. K. Schwarz, *Sci. Rep.* **3**, 1514 (2013).
10. J. L. Lefebvre, Y. Zhang, M. Meister, X. Wang, J. R. Sanes, *Development* **135**, 4141–4151 (2008).
11. X. Wang *et al*., *Neuron* **36**, 843–854 (2002).
12. S. Hasegawa *et al*., *Mol. Cell. Neurosci.* **38**, 66–79 (2008).
13. L. Buck, R. Axel, *Cell* **65**, 175–187 (1991).
14. A. Chess, I. Simon, H. Cedar, R. Axel, *Cell* **78**, 823–834 (1994).
15. P. Mombaerts *et al*., *Cell* **87**, 675–686 (1996).
16. L. R. Saraiva *et al*., *Sci. Rep.* **5**, 18178 (2015).
17. L. Tan, Q. Li, X. S. Xie, *Mol. Syst. Biol.* **11**, 844 (2015).
18. S. Esumi *et al*., *Nat. Genet.* **37**, 171–176 (2005).
19. S. Hasegawa *et al*., *Front. Mol. Neurosci.* **5**, 97 (2012).
20. W. V. Chen, T. Maniatis, *Development* **140**, 3297–3302 (2013).
21. T. Hummel *et al*., *Neuron* **37**, 221–231 (2003).
22. D. Hattori *et al*., *Nature* **449**, 223–227 (2007).
23. W. V. Chen *et al*., *Science* **356**, 10.1126/science.aal3231 (2017).

ACKNOWLEDGMENTS

We thank R. Axel and S. Lomvardas for generously providing mouse lines and reagents and R. Axel, S. Lomvardas, and C. Zuker for their advice and critical input throughout the course of this project and their critical reading and advice on the manuscript. D. Canzio, P. Kratsios, W. Grueber, and members of the Maniatis laboratory also provided critical reading of the manuscript. We thank G. Barnea for the MOR28 antibody and L. Tan, Q. Li, and X. S. Xie for sharing their single-cell OSN RNA-sequencing data. D. Kato provided assistance with the behavioral assay, and excellent technical and mouse support was provided by A. Struve, M. Mendelsohn, and A. Kirner. This work was supported by NIH grant R01N5088476. The supplement contains additional data.

SUPPLEMENTARY MATERIALS

www.sciencemag.org/content/356/6336/411/suppl/DC1
Materials and Methods
Figs. S1 to S16
Tables S1 and S2
References (*24*–*33*)

11 November 2016; accepted 16 February 2017
10.1126/science.aai8801